Catalysts **2015**, *5*, 2147-2160; doi:10.3390/catal5042147

OPEN ACCESS

catalysts

ISSN 2073-4344

www.mdpi.com/journal/catalysts

Article

Jet-Fuel Range Hydrocarbons from Biomass-Derived Sorbitol over Ni-HZSM-5/SBA-15 Catalyst

Yujing Weng [1,2], Songbai Qiu [1], Longlong Ma [1], Qiying Liu [1], Mingyue Ding [1], Qian Zhang [1,2], Qi Zhang [1] and Tiejun Wang [1,*]

[1] Key Laboratory of Renewable Energy, Guangzhou Institute of Energy Conversion, Chinese Academy of Sciences, Guangzhou 510640, China; E-Mails: wengyj@ms.giec.ac.cn (Y.W.); qiusb@ms.giec.ac.cn (S.Q.); mall@ms.giec.ac.cn (L.M.); liuqy@ms.giec.ac.cn (Q.L.); dingmy@ms.giec.ac.cn (M.D.); zhangqian@ms.giec.ac.cn (Q.Z.); zhangqi@ms.giec.ac.cn (Q.Z.)

[2] University of Chinese Academy of Sciences, Beijing 100049, China

* Author to whom correspondence should be addressed; E-Mail: wangtj@ms.giec.ac.cn; Tel.: +86-20-8705-7751; Fax: +86-20-8705-7789.

Academic Editor: Rafael Luque

Received: 10 November 2015 / Accepted: 8 December 2015 / Published: 15 December 2015

Abstract: Aromatics and cyclic-hydrocarbons are the significant components of jet fuel with high energy-density. However, conventional technologies for bio-fuel production cannot produce these products without further aromatization and isomerization. In this work, renewable liquid fuel with high content of aromatics and cyclic-hydrocarbons was obtained through aqueous catalytic conversion of biomass sorbitol over Ni-HZSM-5/SBA-15 catalyst. Texture characteristics of the catalyst were determined by physisorption of N_2, which indicated its bimodal pore structures were microporous (HZSM-5, pore width: 0.56 nm) and mesoporous (SBA-15, pore width: 8 nm). The surface acidity included weak and strong acid sites, predominantly Lewis type, and was further confirmed by the NH_3-TPD and Py-IR analysis. The catalytic performances were tested in a fixed-bed reactor under the conditions of 593 K, WHSV of 0.75 h^{-1}, GHSV of 2500 h^{-1} and 4.0 MPa of hydrogen pressure, whereby oil yield of 40.4 wt. % with aromatics and cyclic-hydrocarbons content of 80.0% was obtained.

Keywords: sorbitol; aromatic; cyclic-hydrocarbon; long-chain alkane; aqueous catalysis

1. Introduction

Jet fuel has high energy density to maximize aircraft range and a low freezing point to avoid the formation of crystalline wax particles during high-altitude flight [1,2]. Fortunately, these requirements are readily met by branched and cyclic hydrocarbons, and, consequently, these types of fuel are not likely to be displaced for air transportation. Moreover, increasing consumption of jet fuel and anthropogenic CO_2 emissions have led to increasing policy mandates to create biomass-derived hydrocarbons for the jet fuel industry [3,4].

The conventional technologies for biomass-derived jet fuel mainly include hydrodeoxygenation (HDO) of plant oil, HDO of pyrolysis oil, and biomass gasification followed by Fischer-Tropsch (F-T) synthesis. HDO of plant oil is efficient and can produce high-quality distillate fuel, but it is constrained by the cost and availability of triglycerides from either oil-producing plants or algae [4]. F-T synthesis is also effective for producing liquid fuels from coal and natural gas, but it is not appropriate for biomass conversion as it is capital intensive and thus necessitate centralized processing in large facilities [3]. Furthermore, linear alkanes formed by these processes need deep hydrocracking and isomerization to reduce their molecular weight and introduce branching for proper fuel stability [1,5]. Additionally, zeolites such as ZSM-5, Beta and Y were usually used as the catalyst for aromatization as their unique microporous structure and shape selectivity. However, large amount of coke were inevitably formed and resulted in the rapid deactivation of catalyst.

Sorbitol as a key intermediate of biomass derivatives is easily obtained by hydrogenation of glucose or even by direct degradation/hydrogenation of cellulose. Its molecule has high oxygen content, with six hydroxy groups, resulting in low thermal stability and natural hydrophility. Aqueous phase HDO is a catalytic process to remove the total or partial oxygenates from water-soluble biomass-derived oxygenates [4–6]. Recently, it has been widely studied as a promising option for biomass-derived jet fuel [5,7–9]. Here, aqueous phase HDO of sorbitol was established in the fixed-bed reactor over the catalyst of Ni-HZSM-5/SBA-15. The catalyst presented bimodal pore structure that was microporous (HZSM-5, pore width: 0.56nm) and mesoporous (SBA-15, pore width: 8 nm). Moreover, it showed efficient performance in the conversion of biomass large-molecule sorbitol (e.g., sorbitol, diameter: 8.7 nm) into small-molecule hydrocarbons. A maximum yield of 40.4 wt. % of oil product was produced at an elevated temperature (593 K) with aromatic and cyclic-hydrocarbon content of 80.0%. Moreover, the normal temperature (473–623 K) of aqueous phase HDO was lower than that (623–773 K) of traditional aromatization, which would reduce the coke formation and deactivation of catalyst. The final oil production mainly consisted of cycloalkanes, branched-alkanes and aromatics, which is a wonderful crude oil to be used as jet fuel after it is hydrogenated to improve quality (deep deoxygenation/chemical bond saturation).

2. Results and Discussion

2.1. Catalyst Characterization

Table 1 summarizes the physicochemical properties of applied catalysts. HZSM-5 contained 1.0 nm elliptical straight channels (0.51 nm × 0.55 nm) and 1.2 nm circular sinusoidal channels (0.53 nm × 0.56 nm) that perpendicularly intersect, which leads to the shape selectivity for cyclic and

branched hydrocarbons such as aromatics and cycloalkanes (Figure S1) [10,11]. SBA-15, ordered mesoporous silica material, was mainly a hexagonal array of cylindrical pores (diameter: 7–9 nm) and high BET surface areas (506 m^2/g). The obtained Ni-HZSM-5/SBA-15 catalyst presented two kinds of pores: micropores of HZSM-5 and mesopores of SBA-15, respectively. This was further evidenced by the pore diameter distribution in Figure 1. The micropore pore diameter range was 0.4–0.8 nm and mesoporous pore diameter range was 3.5–6.0 nm. For micropore distribution, the Ni loading expanded the pore volume with high signal intensity, but no change in pore diameter range. There was also no significant change in the distribution of mesoporous pore diameter with only a slight decrease of intensity after Ni loading comparing with the fresh SBA-15. This demonstrated that the impregnation, drying and calcination steps during the preparation of the catalysts had no significant effect on the micropore and mesoporous distribution of HZSM-5 and SBA-15 [7,12–14].

Table 1. Physicochemical property of catalysts.

Samples	A_{BET} (m^2/g) [a]	V_m (cm^3/g) [a]	A_m (m^2/g) [a]	V_{mes} (cm^3/g) [a]	D_p (nm) [a]
HZSM-5	387.4	0.13	310.2	0.19	/
SBA-15	506.0	/	/	0.70	/
Ni-HZSM-5	341.7	0.09	227.2	0.17	17.8(22.5) [b]
Ni-SBA-15	402.0	/	/	0.55	6.1(9.3) [b]
Ni-HZSM-5/SBA-15	397.7	0.07	151.5	0.45	16.3(21.0) [b]

[a] A_{BET} apparent surface area; V_m micropore volume; A_m micropore surface area; V_{mes} mesopore volume; D_p average particle size, calculated by Scherer's equation, the Bragg angle of 2θ using 43.3°; [b] Particle size was observed by TEM.

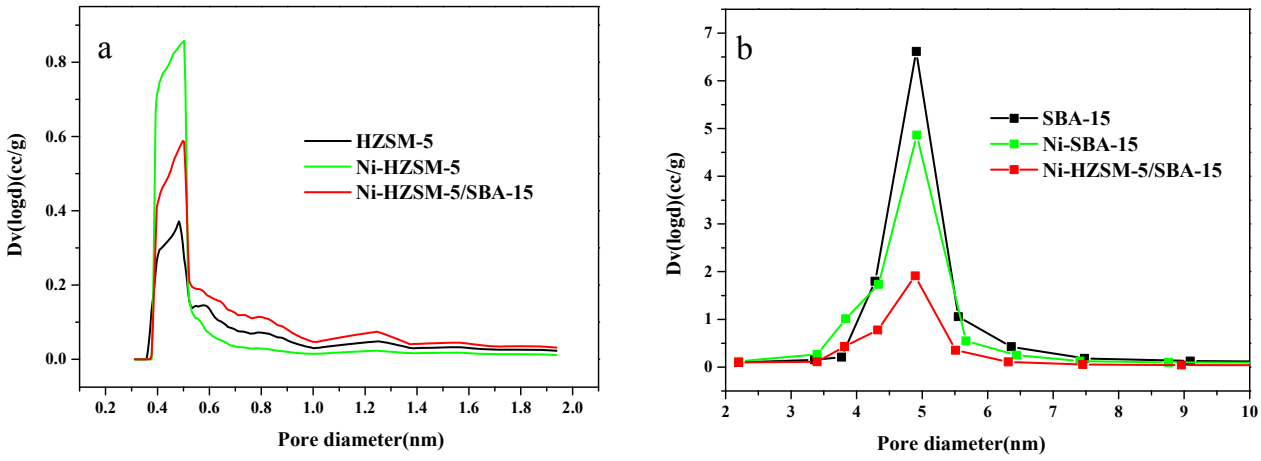

Figure 1. Pore diameter distribution of catalysts in (**a**) micropores; (**b**) mesopores.

Figure 2 represented the X-ray diffractogram of catalysts synthesized from HZSM-5 and SBA-15. The peaks (Figure 2a) at 2θ of 7.9°, 8.7°, 23.0° and 23.9° were attributed to the ZSM-5 zeolite crystal structure [15,16]. Slight attenuation was found on the peak intensity corresponding to Ni-HZSM-5/SBA-15. Moreover, the diffraction peaks at 2θ of 37.5°, 43.4° and 63.2° corresponded to [111], [200] and [220] crystal faces of NiO, respectively. XRD patterns of the samples gave weak and broad peaks to NiO, indicating that NiO particles were very small and highly dispersed on the supports [17]. In small-angle XRD patterns (Figure 2b), SBA-15 presented three peaks, indexed as

(100), (110) and (200) reflections associated with P6mm hexagonal symmetry [18]. Intensities of diffraction peaks were increased and the peak positions were shifted to higher 2θ value for Ni-SBA-15 in comparison to the parent SBA-15. The representative SEM and TEM images of catalysts were shown in Figure 3. The dark spots presented in the images indicated good dispersion of NiO nanoparticles on the supports.

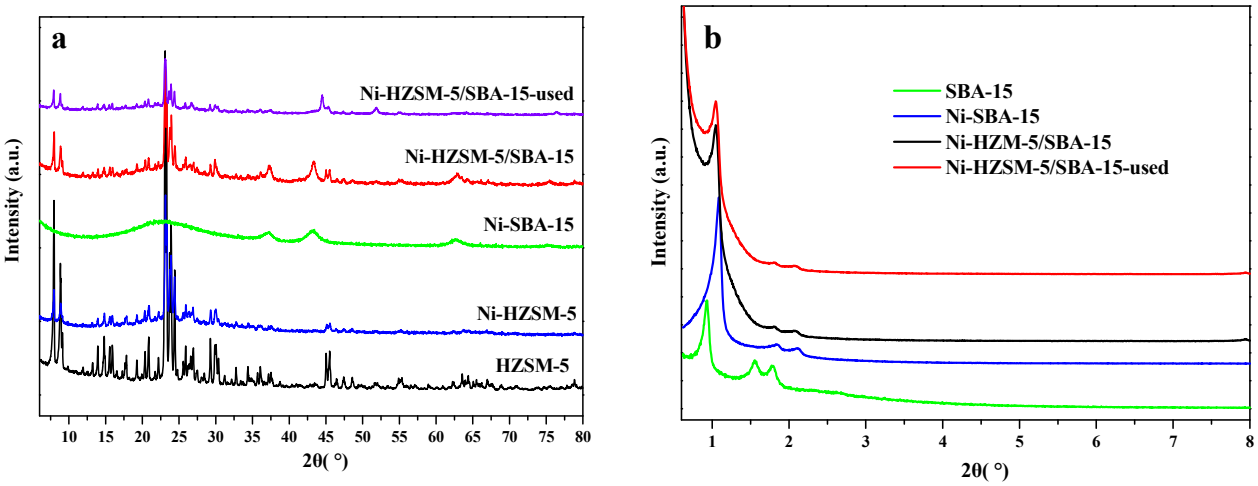

Figure 2. (**a**) Wide-angle XRD patterns of catalysts; (**b**) small-angle XRD patterns of catalysts.

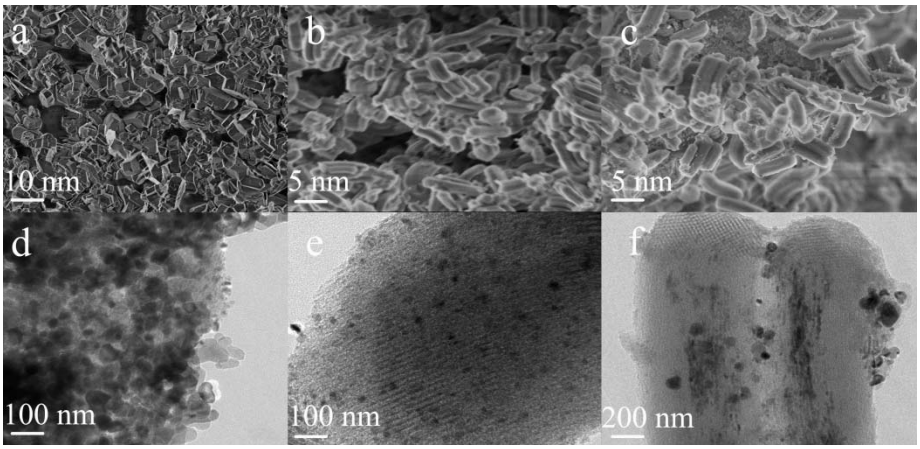

Figure 3. (**a**) SEM images of HZSM-5; (**b**) SEM images SBA-15; (**c**) SEM images Ni-HZSM-5/SBA-15; (**d**) TEM images of Ni/HZM-5; (**e**) TEM images of Ni/SBA-15; (**f**) TEM images of Ni-HZSM-5/SBA-15.

Ammonia can be used as a probe molecule to explore the overall acid properties of the catalyst surface using temperature-programmed desorption (TPD). Thus, NH_3-TPD profiles for the tested catalysts (Figure 4) showed strong and weak acid sites with different acid strengths. The one at 373–550 K could be attributed to the weak adsorption of the NH_3 on the Brønsted acid sites and NH_3 association with Si–OH group [15,19], and the other peak at 550–820 K could be ascribed to strong desorption of NH_3 adsorbed on the acidic Al–OH, Al–OH–Si in the surface and structure [12,15]. The amount of NH_3 adsorption over Ni-HZSM-5 was less than that over HZSM-5, but the doping of Ni strengthened the strong acid sites. Moreover, the addition of SBA-15 decreased the total acid amount of Ni-HZSM-5 [20].

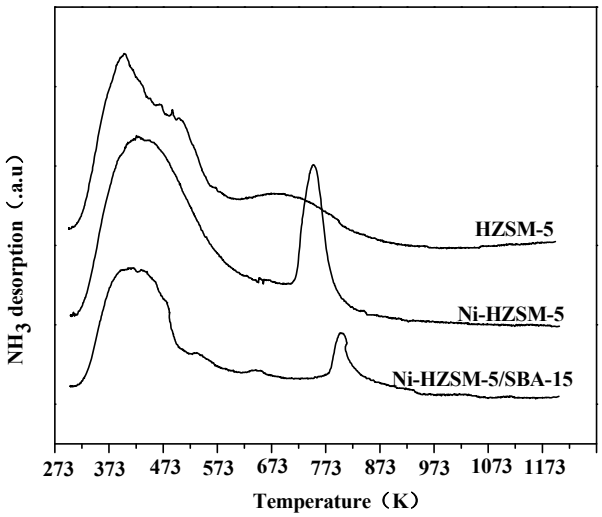

Figure 4. NH_3-TPD analysis of different nickel catalysts.

To further investigate the percentage of Brønsted (B) and Lewis (L) acid sites in the total number of acid sites, the catalysts were measured by Py-IR spectroscopy at 373 and 573 K. The IR band around 1450 cm^{-1} was attributed to the adsorption of pyridine coordinated on Lewis acid sites, and the IR band around 1540 cm^{-1} was associated with the vibration of the pyridinic ring on Brønsted acid sites [15,21,22]. The acidity of these catalysts obtained by Py-IR was summarized in Table 2. Brønsted and Lewis acid sites detected at low temperature (373 K) are attributed to the weak acid sites, and those observed at high temperature (573 K) are assigned to the strong acid sites [23]. From the results obtained by Py-IR for a series of catalyst samples, it can be indicated that the doping of Ni improved the amount of Lewis acid sites of catalyst (Ni-HZSM-5) in relation to original zeolite (HZSM-5). Moreover, the addition of SBA-15 decreased the ratio of B acid sites to L acid sites of Ni-HZSM-5/SBA-15 in relation to Ni-HZSM-5.

Table 2. Acidity of these catalysts obtained by Py-IR.

Samples	373 K [a]		573 K [a]	
	B (mmol/g)	L (mmol/g)	B (mmol/g)	L (mmol/g)
Ni-SBA-15 [b]	0.00	0.01	0.00	0.00
HZSM-5	0.28	0.05	0.19	0.02
Ni-HZSM-5	0.08	0.29	0.04	0.17
Ni-HZSM-5/SBA-15	0.02	0.15	0.01	0.08

[a] 373 and 573 K were the desorption temperatures of pyridine (Py); [b] SBA-15 was pure silica material with little acidity.

Figure 5 presented the FTIR spectra at 573 K of different nickel catalysts after adsorption of pyridine (Py). For pure HZSM-5, the IR band at 1540 cm^{-1} is associated with pyridine adsorption on Brønsted acid sites, which were generally assigned to the framework Al in HZSM-5. In addition, the band at 1488 cm^{-1} was ascribed to the vibration of the pyridine ring on Brønsted and Lewis acid sites. After doping of Ni, the Brønsted acid sites were greatly reduced and Lewis acid sites were largely maintained. Combined with the increased desorption peak centered around 773 K in NH_3-TPD curves (Figure 4), it can be deduced that Ni cations preferentially replace the high-strength Brønsted acid sites

of HZSM-5. For catalyst of Ni-HZSM-5/SBA-15, the Brønsted acid sites nearly disappeared and Lewis acid sites decreased slightly in relation to Ni-HZSM-5.

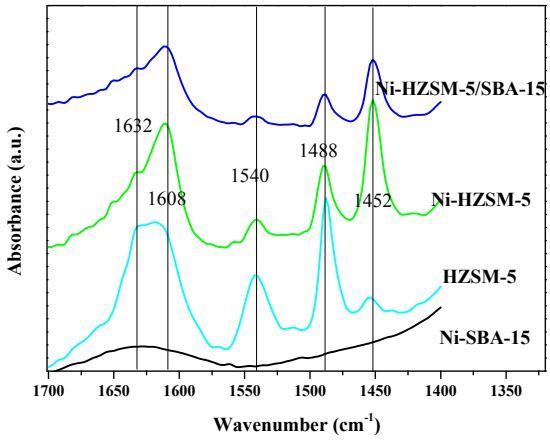

Figure 5. FTIR spectra at 573 K of different nickel catalysts after adsorption of pyridine (Py).

2.2. Products of Sorbitol Transformation

As previously mentioned, the zeolite HZSM-5 have been mechanically mixed with other porous materials for transformation of biomass large-molecule oxygenates (e.g., sorbitol: 0.8 × 0.9 nm), which are unable to enter the micropore of HZSM-5. Zhang and Xiao reported that LOSA-1 (similar to ZSM-5) mixed with γ-Al_2O_3, CaO and MCM-41 had efficient catalytic activity on biomass-derived oxygenates conversion into hydrocarbons. The microporous and mesoporous mixed catalysts were proposed with a significant ability to crack the large-molecule oxygenates into small-molecule oxygenates through the strong cracking characteristic of the adding materials [24].

Here, Ni-HZSM-5/SBA-15 was investigated for sorbitol transformation. Interestingly, the final products in the oil phase were mainly aromatics and cycloalkanes. To study the catalytic mechanism of mixed catalyst, various catalysts were tested in the same reaction condition (Table 3). Single HZSM-5 obtained high isosorbide yield (56.9%) in the aqueous-phase and small amount alkane (9.6%) in the gas-phase. However, isosorbide yield decreased to 7.9% for Ni-HZSM-5 with increasing yield of alkane (40.1%) and oil-phase production (22.4%). This may be attributed to the increase amount of strong Lewis acid sites according to the NH_3-TPD and Py-IR analysis. The main products in the oil-phase were aromatics (78.9%), in accordance with previous reports about Ni-HZSM-5 [16,19,25]. Ni-SBA-15 was tested with high isosorbide yield (30.4%) and a low amount (12.3%) of oil production, which were mainly cycloalkanes and branched-alkanes, indicating the high reforming performance of catalyst. Despite all catalysts showing high performance for sorbitol conversion, the oil yield of Ni@HZSM-5/SBA-15 was significantly increased to 40.4% with high selectivity to cycloalkanes and aromatics. Meanwhile, the gas-phase and aqueous-phase products were remarkably reduced to 24.9% and 21.3%, respectively. Elemental analysis of oil samples with vario EL III elemental analyzer were showed in Table 4. Comparing with the oxygen content (O%) of Ni-HZSM-5 (8.5%), the content of Ni-HZSM-5/SBA-15 (3.4%) decreased greatly, indicating the fact that the HDO performance of catalyst was increased by the addition of SBA-15. The C/H weight ratio (8.6) of oil over Ni-HZSM-5/SBA-15 is lower than that (8.9) over Ni/HZSM-5. This could be explained by the fact that

the main products of Ni-HZSM-5/SBA-15 were not only aromatics, but also more saturated alkanes, whose C/H ratio is lower than that of unsaturated aromatics. According to NH_3-TPD analysis, the decrease of total acid sites of Ni@HZSM-5/SBA-15 restrained the formation of aromatic products and promoted the formation of more saturated alkanes and cycloalkanes [26–28].

Table 3. Product distribution over different catalysts.

Products (%)	HZSM-5	Ni-HZSM-5	Ni-SBA-15	Ni-HZSM-5/SBA-15
Over yields				
CO	/	6.2	1.9	0.6
CO_2	/	1.9	2.1	2.8
C1-C6 alkanes	9.6	40.1	9.9	21.5
Isosorbide	56.9	7.9	30.4	3.2
Ethanol	3.1	1.3	6.5	2.5
2-Pentanone	4.2	3.6	3.6	3.1
2-Hexanone	/	1.0	1.2	1.3
3-Hexanone	/	/	0.9	0.7
2-Methyl-cyclopentanone	/	1.2	2.0	4.3
2-Ehyl-furan	6.5	4.3	3.8	3.2
2,5-Dimethyl-furan	3.3	3.6	3.4	3.0
Oil	/	22.4	12.3	40.4
Total balance	86.6	93.5	70.9	85.6
Unidentified	16.4	6.5	22.0	14.4
Alkane selectivity				
C1	/	7.3	1.4	35.7
C2	0.9	11.5	1.1	3.1
C3	14.0	18.7	2.0	10.4
C4	14.0	25.0	20.7	13.9
C5	64.1	12.4	61.0	22.2
C6	7.0	25.1	6.6	14.6
Oil selectivity				
Toluene	/	8.9	3.6	4.7
Xylenes	/	19.2	4.0	20.3
Alkylbenzenes	/	20.5	6.0	15.9
Indenes	/	10.1	/	8.6
Naphthalenes	/	20.2	/	20.2
Decane	/	/	4.3	0.1
Undecane	/	/	4.1	0.7
Dodecane	/	/	6.1	1.1
Branched-alkanes	/	0.5	10.5	3.1
Methyl-cyclopentane	/	4.0	19.8	5.9
Cyclohexane		2.0	16.2	1.1
Methyl-cyclohexane		1.6	12.1	1.0
Ethyl-cyclohexane		0.5	9.6	2.3
Oxy-compounds	/	10.2	13.0	11.7
Others	/	2.0	9.6	3.3

Reaction condition: 593 K, WHSV of 0.75 h^{-1}, GHSV of 2500 h^{-1} and 4.0 MPa, sorbitol solution 40 wt. %; "/" Trace amount.

Table 4. Elemental analysis of oil products with vario EL III elemental analyzer.

Catalyst	C%	H%	O%	C:H
Ni-HZSM-5	80.4	9.0	9.6	8.9
Ni@HZSM-5/SBA-15	86.5	10.1	3.4	8.6

Figure 6 showed the sorbitol conversion and oil yield as the function of reaction time. Sorbitol conversion remained above 90% during the whole reaction and obtained stable oil phase yield until the reaction time after 70 h. The later slight decrease of oil yield could be attributed to the carbon deposition of organic compounds and aggregation of Ni particles on the surface of the catalyst. According to the TG (Figure S2) analysis, the weight loss was about 4% for the pristine catalyst at about 373 K, which is attributed to the removal of absorbed water. Comparatively, the catalyst after 100 h of reaction presented total weight loss of about 9%, which was due to the removal of water (373 K), the decomposition of organic compounds (653 K), and the deposited carbon combustion (803 K). The covering of organic compounds and carbon deposition probably induced the deactivation of the catalyst.

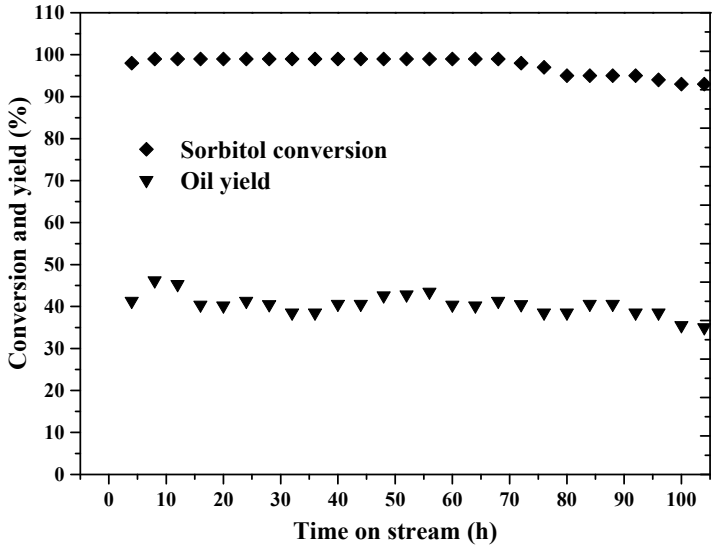

Figure 6. Sorbitol conversion and oil yield as the function of reaction time. Reaction conditions: 20 wt. % sorbitol aqueous solution, 593 K, 4 MPa H_2 pressure, 4 g catalyst.

2.3. Reaction Network

To selectively make jet fuel range compounds from biomass, the microporous and mesoporous structure were adjusted at the bifunctional catalyst (Ni-HZSM-5/SBA-15). As shown in Figure 7, the large sorbitol molecule was firstly hydrodeoxygenated (HDO) to produce some smaller oxy-compounds by the catalysis of Ni-SBA-15. These oxy-compounds included isosorbide, ethanol, 2-pentanone, 2-hexanone, 3-hexanone, 2-methyl-cyclopentanone, 2-ehyl-furan, 2, 5-dimethyl-furan and so on. Table S1 presents the dimension of biomass feedstocks and products from the aqueous catalytic process. Most intermediates enabled entry into the micropore of HZSM-5 for further transformation. The further transformation of sorbitol occurs through five key reaction classes: (1) hydrogenation of C–O–C, C=C, and C=O groups on metal catalytic sites to produce

mono-oxygenated intermediates; (2) C–O bond cleavage on Brønsted-acid catalytic sites to produce cycloalkanes and alkanes; (3) C–C bond cleavage by dehydrogenation, decarbonylation and retro-aldol condensation on metal catalytic sites to produce short chain alkanes; (4) C–C bond coupling by ketonization and aldol-condensation on strong Lewis acid sites to produce long-chain alkanes; and (5) aromatic rings formed by shape-selective effects on ZSM-5 microporous [5,28–30]. The final oil production mainly consisted of cycloalkanes, branched-alkanes and aromatics, which was a wonderful crude oil to be used as jet fuel after it was hydrogenated to improve quality (deep deoxygenation/chemical bond saturation) [1,31,32].

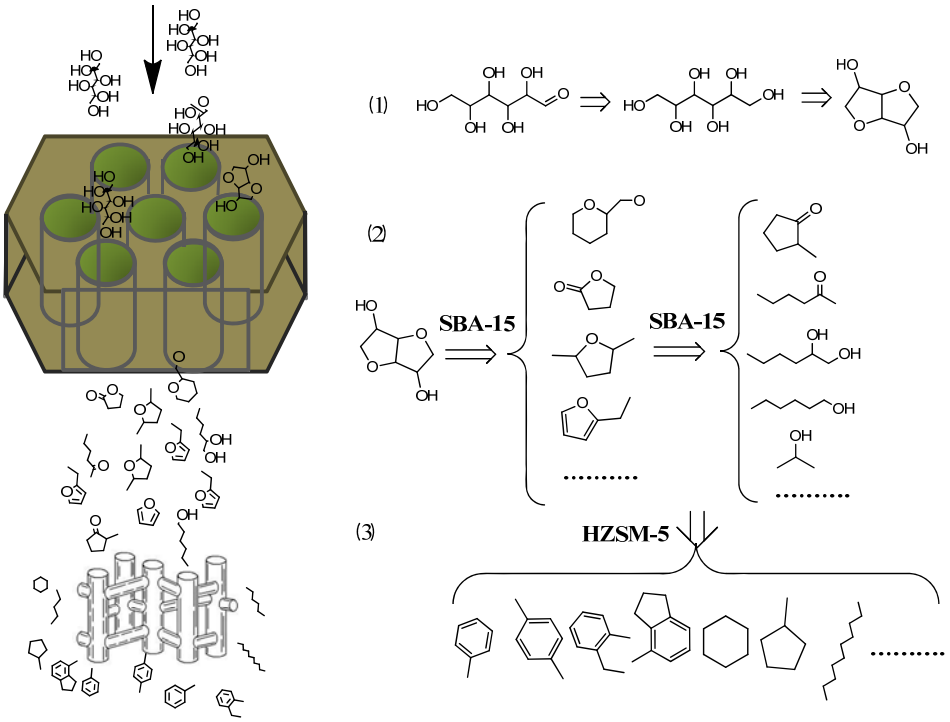

Figure 7. Reaction scheme for biomass-derived sorbitol into liquid fuel.

3. Experimental Section

3.1. Catalyst Preparation

HZSM-5 (Si/Al = 38, Nankai University catalyst Co., Ltd., Tianjin, China), SBA-15 (Si/Al = ∞, Nanjing Xfnano Co., Ltd., Nanjing, China) were selected as support materials. All of the catalysts were synthesized by the method reported before [17,33]. Ni-HZSM-5, Ni-SBA-15 were prepared by wet impregnation method with nickel nitrate ($Ni(NO_3)_2 \cdot 6H_2O$) [34]. Firstly, appropriate amount of carrier (HZSM-5 or SBA-15) grains were impregnated with aqueous solution of $Ni(NO_3)_2 \cdot 6H_2O$ at 313 K for 12 h, followed by drying in air overnight, and then calcined at 823 K for 4 h. The metal Ni loading on the catalysts was 10 wt. %. The Ni-HZSM-5/SBA-15 was prepared by mixing the Ni/HZSM-5 sample with Ni/SBA-15 sample (1:1 by mass). Subsequently, the mixture was ground into slurry by adding an appropriate amount of deionized water. Then, the obtained slurry was stirred, dried and calcined under the conditions motioned above. Prior to the reaction, all of the catalysts were reduced by a flow of H_2 (50 mL/min) at 450 °C for 4 h.

3.2. Catalyst Characterization

The BET surface area and pore volume of catalysts were determined by nitrogen adsorption at 77 K using a QUADRASORB SI analyzer equipped with QuadraWin software system (Quantachrome, Boynton Beach, FL, USA). The mesoporous pore volume was calculated with the BJH method and the micropore volume was calculated with the HK method. The crystalline structure of the catalysts was characterized by X-ray diffraction (XRD) (X Pert Pro MPD with Cu Kα (λ = 0.154 nm) radiation, PANalytical, Almelo, The Netherlands) operated at 40 kV and 100 mA. Scanning angle (2θ) ranged from 5° to 80°. Small angle X-ray diffraction was also performed in the range of 2θ from 0.5° to 10°. Additionally, scanning electron microscopy (SEM, Zeiss, Jena, Germany), transmission electron microscopy (TEM, Tokyo, Japan) and SEM-EDS were also used to study the textural properties, phase compositions, and morphologies of the catalysts. NH_3 temperature-programmed desorption (NH_3-TPD) with a Micromeritics chemisorbs 2750 pulse chemisorption system was used to estimate the acidity (150 mg catalyst). The sample was firstly pre-treated by helium flow (30 $cm^3 \cdot min^{-1}$) at 573 K for 1 h, and then cooled to 303 K and ammonia-saturated in a stream of 10% NH_3/He flow (50 $mL \cdot min^{-1}$) for 1 h. The desorption of NH_3 was carried out in helium gas flow (30 $cm^3 \cdot min^{-1}$) by increasing the temperature from room temperature to 1223 K at the heating rate of 10 $K \cdot min^{-1}$. The desorbed ammonia was analyzed by a thermal conduct detector (TCD) [10,35]. Infrared spectra of pyridine adsorption (FTIR-Py) were recorded on a Thermo Nicolet Nexus FT-IR spectrometer (Waltham, MA, USA) equipped with a liquid nitrogen cooled MCT detector. The catalyst samples were firstly pressed into a self-supported wafer and treated at 673 K in an *in situ* IR cell for 0.5 h, and then followed by cooling to 323 K under vacuum to record the background spectra of the cell and the sample wafer. Next, these samples were exposed to pyridine vapor for 10 min and evacuated at the appointed temperature to remove physical adsorbed pyridine. The spectra were recorded in the range of 1700–1400 cm^{-1} with 32 scans and a resolution of 4 cm^{-1} [36]. Thermal behavior of catalysts before and after reaction was examined by non-isothermal thermogravimetric analysis (TGA) with a Mettler Toledo instrument (TGA /SDTA851e, Bavaria, Germany). Thermogravimetirc (TG) and differential thermogravimetric (DTG) curves were recorded from 323 K to 1073 K at a heating rate of 20 K/min, under an air atmosphere.

3.3. Catalyst Tests

Fixed-bed reaction (Figure S3) was carried out in a tubular stainless steel fixed-bed reactor (inner diameter of 10 mm; length of 350 mm) at 4 MPa H_2 pressure. Before the reaction, 4 mL catalyst (≈1.5 g) was loaded in the constant temperature zone of the reactor with quartz sand and quartz wool as the filler materials on the top and bottom of the catalyst bed, respectively. During reaction, the sorbitol solution (40 wt. %) was pumped into the fixed-bed reactor at the flow rate of 0.05 mL/min by a high pressure liquid pump (HPLP). H_2 flow (150 mL/min) was purged into the reactor at the same time. The fixed reactor set-up kept H_2 pressure at 4 MPa with the use of pre-pressure controller and rear pressure, and operated in the co-current-flow of liquid and hydrogen from top to bottom.

3.4. Product Analysis

Gaseous samples were collected with a gasbag and verified as alkane through the external standard method by Agilent GC-7890A gas chromatograph (GS-Gas Pro capillary column, 60 m × 0.32 mm, ±5%, Santa Clara, CA, USA) equipped with a thermal conduct detector (TCD) and a flame ionization detector (FID). Liquid samples (oil and aqueous phase), were condensed and collected in an ice-water condensing tank and then weighted at Analytical Balance (±0.5%). The components in aqueous phase was detected and quantified by Waters Alliance e2695 HPLC (±2.27%, Milford, MA, USA) with UV-Vis (Waters 2489, Milford, MA, USA) and Refractometer (Waters 2414, Milford, MA, USA) detector by using a Shodex SH1011 column (8 × 300 mm, New York, NY, USA). 0.005 M H_2SO_4 as mobile phase flowed at a rate of 0.5 mL·min^{-1}. GC-MS (Thermo Trace GC Ultra with a PolarisQ ion trap mass spectrometer, Waltham, MA, USA) equipped with a HP-INOWx capillary column was applied to analyze the species in aqueous samples and a HP-5MScapillary column was applied to analyze the species in the oil phase samples. Total carbon content and C/H weight ratio in the liquid products were measured by a Vario EL III elemental analyzer. The sorbitol conversion, product yield, and selectivity were measured by the definition equations listed below. $C_{\text{sorbitol,inlet}}$ and $C_{\text{sorbitol,aqueous}}$ are the concentration of feedstock at the inlet and outlet, respectively; C_{product} is the concentration of carbon in the product at the corresponding phase; and V is the corresponding phase volume. Product carbon selectivity was defined as the ratio of carbon moles of product divided by the total carbon moles of corresponding categories.

$$\text{Conversion}(\%) = \frac{C_{\text{sorbitol, inlet}} V_{\text{inlet}} - C_{\text{sorbitol,aqueous}} V_{\text{aqueous}}}{C_{\text{sorbitol,inlet}} V_{\text{inlet}}} \times 100 \quad (1)$$

$$\text{Yield}(\%) = \frac{C_{\text{product,aqueous}} V_{\text{aqueous}} + C_{\text{product,orgainc}} V_{\text{organic}} + C_{\text{product,gaseous}} V_{\text{gaseous}}}{C_{\text{sorbitol,inlet}} V_{\text{inlet}}} \times 100 \quad (2)$$

$$\text{Selectivity}(\%) = \frac{C_{\text{product}} V_i}{\sum_{i=1}^{n} C_{\text{product}} V_i} \times 100 \quad (3)$$

4. Conclusions

In this work, renewable liquid fuels with high content of aromatics and cyclic-hydrocarbons were obtained by aqueous phase catalytic conversion of biomass sorbitol over the Ni@HZSM-5/SBA-15 catalyst. The catalyst presented bimodal pore structure and efficient performance in the conversion of biomass large-molecule sorbitol (e.g., sorbitol, diameter: 8.7 nm) into small-molecule hydrocarbons. Maximum oil hydrocarbons yield of 40.4 wt. % with aromatics and cyclic-hydrocarbons content of 80.0% was obtained at 593 K, which was lower than that (623–773 K) of traditional aromatization. The produced hydrocarbons are mainly cycloalkanes, branched-alkanes and aromatics, which are wonderful crude oils to be used as jet fuel after being hydrogenated to improve quality (deep deoxygenation/chemical bond saturation).

Acknowledgments

This work was supported by grants from the National Natural Science Foundation of China (No. 51476176&21306195), the National 863 Plan (No. 2012AA101806) and China-EU SMEs Cooperation Fund for energy conservation research project (NO. SQ2013ZOB000002).

Author Contributions

Y.W., S.Q., L.M. and T.W. designed the experiments. Y.W., S.Q., and Q.Z. conducted the experiments. S.Q., Q.L., and M.D. analyzed the data. Y.W. wrote the first draft of the manuscript which was then revised by all other authors.

Conflicts of Interest

The authors declare no conflict of interest.

References

1. Wang, T.; Qiu, S.; Weng, Y.; Chen, L.; Liu, Q.; Long, J.; Tan, J.; Zhang, Q.; Zhang, Q.; Ma, L. Liquid fuel production by aqueous phase catalytic transformation of biomass for aviation. *Appl. Energy* **2015**, *160*, 329–335.
2. Sacia, E.R.; Balakrishnan, M.; Deaner, M.H.; Goulas, K.A.; Toste, F.D.; Bell, A.T. Highly selective condensation of biomass-derived methyl ketones as a source of aviation fuel. *ChemSusChem* **2015**, *8*, 1726–1736.
3. Pant, H.A.Z.A.K.K. Activity of Oxalic Acid Treated ZnO–CuO-HZSM-5 Catalyst for the Transformation of Methanol to Gasoline Range Hydrocarbons. *Ind. Eng. Chem. Res.* **2008**, *47*, 2970–2975.
4. Grilc, M.; Veryasov, G.; Likozar, B.; Jesih, A.; Levec, J. Hydrodeoxygenation of solvolysed lignocellulosic biomass by unsupported MoS_2, MoO_2, Mo_2C and WS_2 catalysts. *Appl. Catal. B* **2015**, *163*, 467–477.
5. Kim, Y.T.; Dumesic, J.A.; Huber, G.W. Aqueous-phase hydrodeoxygenation of sorbitol: A comparative study of Pt/Zr phosphate and $PtReO_x$/C. *J. Catal.* **2013**, *304*, 72–85.
6. Dietrich, P.J.; Lobo-Lapidus, R.J.; Wu, T.P.; Sumer, A.; Akatay, M.C.; Fingland, B.R.; Guo, N.; Dumesic, J.A.; Marshall, C.L.; Stach, E.; *et al*. Aqueous Phase Glycerol Reforming by PtMo Bimetallic Nano-Particle Catalyst: Product Selectivity and Structural Characterization. *Top. Catal.* **2012**, *55*, 53–69.
7. Kirilin, A.V.; Tokarev, A.V.; Kustov, L.M.; Salmi, T.; Mikkola, J.P.; Murzin, D.Y. Aqueous phase reforming of xylitol and sorbitol: Comparison and influence of substrate structure. *Appl. Catal. A* **2012**, *435*, 172–180.
8. Zhang, Q.; Wang, T.; Li, B.; Jiang, T.; Ma, L.; Zhang, X.; Liu, Q. Aqueous phase reforming of sorbitol to bio-gasoline over Ni/HZSM-5 catalysts. *Appl. Energy* **2012**, *97*, 509–513.
9. Li, N.; Huber, G.W. Aqueous-phase hydrodeoxygenation of sorbitol with Pt/SiO_2–Al_2O_3: Identification of reaction intermediates. *J. Catal.* **2010**, *270*, 48–59.

10. Zhu, Z.; Chen, Q.; Xie, Z.; Yang, W.; Li, C. The roles of acidity and structure of zeolite for catalyzing toluene alkylation with methanol to xylene. *Microporous Mesoporous Mater.* **2006**, *88*, 16–21.
11. Bowen, T.C.; Noble, R.D.; Falconer, J.L. Fundamentals and applications of pervaporation through zeolite membranes. *J. Membr. Sci.* **2004**, *245*, 1–33.
12. Zheng, A.; Zhao, Z.; Chang, S.; Huang, Z.; Zhao, K.; Wu, H.; Wang, X.; He, F.; Li, H. Maximum synergistic effect in the coupling conversion of bio-derived furans and methanol over ZSM-5 for enhancing aromatic production. *Green Chem.* **2014**, *16*, 2580–2586.
13. Street, J.; Yu, F.; Wooten, J.; Columbus, E.; White, M.G.; Warnock, J. Gasoline-range hydrocarbon production using biomass derived synthesis gas over Mo/H+ZSM-5. *Fuel* **2012**, *96*, 239–249.
14. Simonetti, D.A.; Kunkes, E.L.; Dumesic, J.A. Gas-phase conversion of glycerol to synthesis gas over carbon-supported platinum and platinum-rhenium catalysts. *J. Catal.* **2007**, *247*, 298–306.
15. Hoang, T.Q.; Zhu, X.; Lobban, L.L.; Resasco, D.E.; Mallinson, R.G. Effects of HZSM-5 crystallite size on stability and alkyl-aromatics product distribution from conversion of propanal. *Catal. Commun.* **2010**, *11*, 977–981.
16. Yin, C.; Zhao, R.; Liu, C. Transformation of olefin over Ni/HZSM-5 catalyst. *Fuel* **2005**, *84*, 701–706.
17. Qiu, S.; Zhang, X.; Liu, Q.; Wang, T.; Zhang, Q.; Ma, L. A simple method to prepare highly active and dispersed Ni/MCM-41 catalysts by co-impregnation. *Catal. Commun.* **2013**, *42*, 73–78.
18. Krishnan, C.K.; Nakamura, K.; Hirata, H.; Ogura, M. Pt/CeO_2–ZrO_2 present in the mesopores of SBA-15—A better catalyst for CO oxidation. *Phys. Chem. Chem. Phys.* **2010**, *12*, 7513–7520.
19. Hoang, T.Q.; Zhu, X.; Danuthai, T.; Lobban, L.L.; Resasco, D.E.; Mallinson, R.G. Conversion of Glycerol to Alkyl-aromatics over Zeolites. *Energy Fuels* **2010**, *24*, 3804–3809.
20. Murata, M.I.K.; Takahara, I. Effects of surface modification of HZSM-5 catalysts on direct transformation of ethanol into lower olefins. *J. Jpn. Pet. Inst.* **2008**, *51*, 234–239.
21. Zhu, X.; Lobban, L.L.; Mallinson, R.G.; Resasco, D.E. Tailoring the mesopore structure of HZSM-5 to control product distribution in the conversion of propanal. *J. Catal.* **2010**, *271*, 88–98.
22. Zhao, Y.; Pan, T.; Zuo, Y.; Guo, Q.X.; Fu, Y. Production of aromatic hydrocarbons through catalytic pyrolysis of 5-hydroxymethylfurfural from biomass. *Bioresour. Technol.* **2013**, *147*, 37–42.
23. Zhang, X.; Zhong, J.; Wang, J.; Zhang, L.; Gao, J.; Liu, A. Catalytic performance and characterization of Ni-doped HZSM-5 catalysts for selective trimerization of *n*-butene. *Fuel Process. Technol.* **2009**, *90*, 863–870.
24. Zhang, H.; Xiao, R.; Jin, B.; Xiao, G.; Chen, R. Biomass catalytic pyrolysis to produce olefins and aromatics with a physically mixed catalyst. *Bioresour. Technol.* **2013**, *140*, 256–262.
25. Jiang, T.; Wang, T.J.; Ma, L.L.; Li, Y.P.; Zhang, Q.; Zhang, X.H. Investigation on the xylitol aqueous-phase reforming performance for pentane production over Pt/HZSM-5 and Ni/HZSM-5 catalysts. *Appl. Energy* **2012**, *90*, 51–57.
26. Wenga, Y.; Qiu, S.; Xu, Y.; Ding, M.; Chen, L.; Zhang, Q.; Ma, L.; Wang, T. One-pot aqueous phase catalytic conversion of sorbitol to gasoline over nickel catalyst. *Energy Convers. Manag.* **2015**, *94*, 95–102.

27. Aguayo, A.T.; Gayubo, A.G.; Atutxa, A.; Valle, B.; Bilbao, J. Regeneration of a HZSM-5 zeolite catalyst deactivated in the transformation of aqueous ethanol into hydrocarbons. *Catal. Today* **2005**, *107–108*, 410–416.
28. Carlson, T.R.; Jae, J.; Lin, Y.-C.; Tompsett, G.A.; Huber, G.W. Catalytic fast pyrolysis of glucose with HZSM-5: The combined homogeneous and heterogeneous reactions. *J. Catal.* **2010**, *270*, 110–124.
29. Vilcocq, L.; Cabiac, A.; Especel, C.; Lacombe, S.; Duprez, D. New insights into the mechanism of sorbitol transformation over an original bifunctional catalytic system. *J. Catal.* **2014**, *320*, 16–25.
30. Kunkes, E.L.; Gurbuz, E.I.; Dumesic, J.A. Vapour-phase C–C coupling reactions of biomass-derived oxygenates over Pd/CeZrO_x catalysts. *J. Catal.* **2009**, *266*, 236–249.
31. Bond, J.Q.; Upadhye, A.A.; Olcay, H.; Tompsett, G.A.; Jae, J.; Xing, R.; Alonso, D.M.; Wang, D.; Zhang, T.; Kumar, R.; *et al*. Production of renewable jet fuel range alkanes and commodity chemicals from integrated catalytic processing of biomass. *Energy Environ. Sci.* **2014**, *7*, 1500–1523.
32. Blommel, P.G.; Keenan, G.R.; Rozmiarek, R.T.; Cortrigth, R.D. Catalytic conversion of sugar into conventional gasoline, diesel, jet fuel, and other hydrocarbons. *Int. Sugar J.* **2008**, *110*, 672–681.
33. Zhang, Q.; Jiang, T.; Li, B.; Wang, T.; Zhang, X.; Zhang, Q.; Ma, L. Highly Selective Sorbitol Hydrogenolysis to Liquid Alkanes over Ni/HZSM-5 Catalysts Modified with Pure Silica MCM-41. *ChemCatChem* **2012**, *4*, 1084–1087.
34. Qiu, S.B.; Weng, Y.J.; Li, Y.P.; Ma, L.L.; Zhang, Q.; Wang, T.J. Promotion of Ni/MCM-41 Catalyst for Hydrogenation of Naphthalene by co-Impregnation with Polyols. *Chin. J. Chem. Phys.* **2014**, *27*, 433–438.
35. Zhang, K.; Liu, Y.; Tian, S.; Zhao, E.; Zhang, J.; Liu, C. Preparation of bifunctional NiPb/ZnO-diatomite-ZSM-5 catalyst and its reactive adsorption desulfurization coupling aromatization performance in FCC gasoline upgrading process. *Fuel* **2013**, *104*, 201–207.
36. Vu, X.H.; Nguyen, S.; Dang, T.T.; Phan, B.M.Q.; Nguyen, D.A.; Armbruster, U.; Martin, A. Catalytic Cracking of Triglyceride-Rich Biomass toward Lower Olefins over a Nano-ZSM-5/SBA-15 Analog Composite. *Catalysts* **2015**, *5*, 1692–1703.